Lunar domes in Mare Undarum: Spectral and morphometric properties, eruption conditions, and mode of emplacement

Raffaello Lena
Via Cartesio 144, sc. D, 00137, Rome, Italy
lena@glrgroup.org

Christian Wöhler
Daimler AG, Group Research, Environment Perception
P. O. Box 2360, D-89013 Ulm, Germany
christian.woehler@daimler.com

Maria Teresa Bregante
Via Antica Romana Occ. 13, 16039, Sestri Levante (Genova), Italy
breterrimar@yahoo.it

Paolo Lazzarotti
Via Pernice 71, 54100 Massa (MS), Italy
paolo@lazzarotti-optics.com

Stefan Lammel
26 Amberley Way, Uxbridge, Middlesex, England
slamm@blueyonder.co.uk

Geologic Lunar Research (GLR) group

Abstract

In this study we examine five lunar domes in Mare Undarum. Four domes termed Condorcet 1–4 are located between the craters Condorcet P and Dubiago, immediately east of Dubiago V and W. The fifth dome, termed Dubiago 3, is located about 35 km further south. The region under study is situated in a major trough concentric to the Crisium basin. The domes Condorcet 1–3 are aligned radially with respect to the Crisium basin. Similar dome configurations aligned radial to major impact basins are known from other lunar mare dome fields. The spectral signature of the domes derived from Clementine UVVIS imagery reveals that they consist of basaltic lava with a low TiO_2 content below 2 wt% and with a FeO content around 10 wt%. Three examined domes exhibit highland components in their soils, which we attribute to lateral mixing between the material in the mare ponds and the surrounding highland material due to random impacts. All five domes have moderate diameters between 10 and 12 km. Condorcet 1–3 are similar to effusive domes of intermediate flank slope between 1° and 2° like those situated in the Hortensius/Milichius/T. Mayer region, while Condorcet 4 has an exceptionally steep flank slope of 2.8° and a large volume. With its low flank slope of 0.9°, the dome Dubiago 3 is morphometrically very similar to a known intrusive dome in the west of Mare Serenitatis. Hence, this structure is possibly of intrusive origin, but with the available data an effusive origin cannot be ruled out. Based on a rheologic model, we infer the physical conditions under which the domes were formed (lava viscosity, effusion rate, magma rise speed) as well as the geometries of the feeder dikes.

Keywords: Moon; volcanism; image processing; spectrophotometry; geological processes

1 Introduction

Mare Undarum, as well as Mare Spumans, Bonitatis, and Anguis, are mare patches outside the main rim of the Crisium impact basin. Mare Undarum is an uneven mare located just north of Mare Spumans on the lunar near side, between Firmicus crater and the eastern limb of the apparent lunar disk. It is centred at selenographic coordinates 68.4° E and 6.8° N, and it is contained within a diameter of 243 km. The crater Dubiago[1] lies on the southern edge of the mare. On the north-eastern edge the crater Condorcet P is situated. A part of Mare Undarum is included in USGS lunar geologic map I-837 (Olson and Wilhelms, 1974), USGS lunar geologic map I-948 (Wilhelms and El-Baz, 1977), and Lunar Map series LM-62. Furthermore, the Lunar Topographic Orthophotomap LTO 63D1 contains an elevation map of the Mare Undarum region. A section of Consolidated Lunar Atlas image D1 (Kuiper et al., 1967) providing an overview about the Mare Undarum region is shown in Fig. 1.

The Crisium basin formed in a period of high cratering flux, dated as 4.05–4.13 Ga (Baldwin, 1974; Nunes et al., 1974; Schaeffer and Husain, 1974). Mare Spumans and Mare Undarum are presumably located within the continuous Crisium ejecta. The surrounding basin material is of Nectarian age, with the mare basalt being of Upper Imbrian age (cf. Olson and Wilhelms (1974) and references therein). Different lithological units, included in USGS lunar geologic map I-837, are apparent in the mapped half of Mare Undarum (cf. Olson and Wilhelms, 1974). In USGS geologic map I-837 the mare basalts comprised between the craters Dubiago and Condorcet P have been mapped as two distinct units, Im1 and Im2. Im units denote flows of volcanic material possibly including some pyroclastic material (Olson and Wilhelms, 1974). The unit Im2 is darker and less cratered than unit Im1 which has a higher albedo possibly caused by a higher fraction of admixed highland material. Hence, unit Im2 is younger than Im1. The major trends of the Spumans-Undarum trough-like basin are attributable to the formation or modification of the Crisium basin north-west of this region (Wilhelms, 1973; Olson and Wilhelms, 1974; Spudis, 1993).

Lunar Orbiter high-resolution image IV-178-H1, acquired at an unusually low illumination angle and providing an oblique view on the eastern half of Mare Undarum, clearly displays five low and smooth elevated structures, which are lunar mare domes (Fig. 2). The domes are situated in an Im1 unit. The presence of such pronounced mare domes appears to be somewhat unexpected in a region so close to the lunar farside, as in the farside maria domes are not abundant. In this study we will perform a detailed examination of these five domes. Based on high-resolution telescopic CCD observations carried out under strongly oblique illumination conditions, we examine their morphometric characteristics by making use of a combined photoclinometry and shape from shading approach (Horn, 1989; Wöhler and Hafezi, 2005; Lena et al., 2006a; Wöhler et al., 2006). The obtained values are used to derive information about the physical parameters of dome formation (lava viscosity, effusion rate, duration of the effusion process, magma rise speed, dike dimensions), employing the rheologic model by Wilson and Head (2003). We provide a geological interpretation of our spectrophotometric,

[1]The spelling "Dubiago" is according to IAU nomenclature, while in the Lunar Topographic Orthophotomap (LTO) and Lunar Orthophotomap (LO) series the spelling "Dubyago" can be found.

morphometric, and rheologic modelling results, comparing them to the corresponding parameters observed for lunar mare domes in the large dome fields situated on the lunar nearside.

2 Geologic setting of the Mare Undarum region

The concentric structure of the Crisium basin consists of a series of raised rings and intervening troughs. Several rugged rings are delineated in the circum-mare highlands, and other rings inside the mare are revealed by concentric wrinkle ridge patterns. Wilhelms (1973) identifies basin rings with diameters of approximately 420, 500, 680, and 970 km. A more recent interpretation of the multi-ring pattern by Spudis (1993) comprises one ring of 360 km diameter inside the mare, which is probably identical with the 420 km ring postulated by Wilhelms (1973), and the mare-bordering 540 km ring. The highland elevations around the abrupt edge of the mare are relatively constant, revealing a further ring of 740 km diameter which is identified by Spudis (1993) as the main topographic ring of the Crisium basin. Two larger, exterior rings of 1080 and 1600 km diameter display a scarp-like morphology and resemble the outer rings of the Nectaris and Imbrium basins.

The raised rings, termed platform massifs by Spudis (1993), are composed of pre-basin rock and overlying basin ejecta. Between the platform massifs, concentric troughs are revealed by the available topographic data (Spudis, 1993), which are filled by debris derived from the raised rings and by younger plains and mare materials (Wilhelms, 1973). No other lunar multi-ring basin displays similar ring troughs. Hence, Spudis (1993) explains those observed around the Crisium basin by internal modification of basin morphology. A comprehensive overview about the Crisium basalts and regional stratigraphy is provided by Head et al. (1978). They identify three groups of soils in Mare Crisium. Group I soils are rich in Mg and FeO and have a moderate TiO_2 content of 3–5 wt%. They were originally emplaced over large regions of the basin and are presently exposed as a shelf in its southwestern part. Group IIa soils have a high FeO content and a low TiO_2 content of about 1–2 wt%. Soils of group IIb are similar but have a lower FeO content. The soils of group II were emplaced in two stages subsequent to those of group I and appear as a part of the outer shelf and the topographic basin rim. Soils of group III occur discontinuously in the centre of Mare Crisium. The TiO_2 content amounts to about 2–3 wt%. Subsidence of the Crisium basin occurred before and after the emplacement of the group III basalts.

According to De Hon (1975), the gross structure of Mare Undarum is characterised by a large trough of 820 km diameter, concentric with respect to Mare Crisium, thus located between the main topographic basin ring of 740 km diameter and the outer 1080 km ring. The cratering sequence occurring in the Mare Undarum region can be divided into three different stages. Stage I craters, formed in a period of high impact flux rate, are highly degraded and blanketed by Crisium ejecta. Stage II craters formed on the mantled surface and are in turn flooded by mare basalts, while stage III craters formed after emplacement of mare basalts during a period of much lower, more or less constant impact rate (Neukum et al., 2001). The impact that formed the Crisium

basin spread ejecta across the area which filled and degraded preexisting stage I craters. De Hon (1975) examines the basalt thickness in Mare Undarum and Mare Spumans relying on measurements of the exposed rim heights of craters partially buried by mare basalt. An isopach map and a reconstruction of the prebasalt surface are provided, indicating that stage II craters developed on the degraded surface until Imbrian basalt flows flooded the low-lying terrain and buried stage I crater remnants and stage II craters. Especially, thick lenses of mare basalt occur in Mare Undarum near the southern rim of Condorcet P, on the north-western rim of Dubiago, and associated with a buried stage I crater at 6° N and 68° E. The average thickness is 200 m with local thickenings of about 900 m (De Hon, 1975; De Hon and Waskom, 1976).

Clark and Hawke (1987) study the geochemical variations in the Undarum/Spumans/Balmer region. All of the mare areas show ranges of concentrations of Al, Mg, Fe, Ti, and Th which indicate the presence of mare basalts. Mare Spumans has a low Al concentration characteristic of typical mare basalt. Mare Undarum is somewhat more aluminous and less mafic, probably indicating contamination with highland debris in basins and ponds (Clark and Hawke, 1982, 1987). Their orbital geochemical data sets indicate that the Mare Undarum region is chemically heterogeneous. Northern and eastern Mare Undarum and parts of Mare Spumans have relatively low MgO contents of 7–7.5 wt% while southern Mare Undarum and eastern Mare Spumans have MgO contents higher than 7.5 wt% which is indicative of more typical mare basalts (Clark and Hawke, 1982, 1987). This variation could be caused by the different extent to which contamination by surrounding highland material has occurred within these areas. The considerable efficiency of this lateral mixing mechanism caused by random impacts is discussed in detail by Li and Mustard (2000, 2005). FeO concentrations are higher than 11.4 wt% in many mare units, including southern Mare Undarum and much of Mare Spumans, and are less than 7.5 wt% in the north-eastern portion of the region, which contains the greatest expanse of highland material (Clark and Hawke, 1987).

Fig. 3 shows that the three domes Condorcet 1–3 are aligned radially with respect to the centre of the Crisium basin. Similar radial alignments of lunar domes with respect to the centres of major impact basins are described by Wöhler et al. (2007).

3 An overview about lunar mare domes

Mare domes are smooth low features with convex profiles gently bent upwards. They are circular to elliptical in shape. Lunar domes are formed either by outpouring of magma from a central vent or by a subsurface accumulation of magma that causes an up-doming of the bedrock layers, creating a smooth, gently sloping positive relief. Domes representing volcanic sources are smooth-surfaced and usually have summit pits or elongated vents, fissures, or pit chains (Wilhelms, 1987). Most vents related to domes appear to be associated with surrounding lava plains of known volcanic origin or in association with pyroclastic deposits (Head and Gifford 1980; Jackson et al., 1997).

Isolated domes may be found in almost all maria, but they are concentrated on the lunar nearside and show significant abundance in the Hortensius region, Oceanus

Procellarum, and in Mare Tranquillitatis. Mare domes are commonly interpreted as shield volcanoes (Wilhelms and McCauley, 1971) or laccoliths (Spurr, 1945; Baldwin, 1963; Wilhelms and McCauley, 1971).

Effusive lunar domes probably formed during the terminal phase of a volcanic eruption. Initially, lunar lavas were very fluid due to their high temperature. Thus, they were able to form extended basaltic mare plains. Over time, the temperature of the erupting lavas became lower, flow rate decreased, and crystallisation occurred. This changed the characteristics of the lava such that it began to "pile up" around the effusion vent and formed a dome (Cattermole, 1996; Mursky, 1996). Weitz and Head (1999) show that steeper domes represent the result of cooler, more viscous lavas with high crystalline content, possibly at the final stages of the eruption. Factors governing the morphological development of volcanic edifices are interrelated, including the viscosity of the erupted material, its temperature, its composition, the duration of the eruption process, the eruption rate, and the number of repeated eruptions from the vent. The viscosity of the magma depends on its temperature and composition, where the amount of crystalline material will depend upon how it is transported from the reservoir to the surface and on the crystallisation temperature of its component phases.

Mare volcanic eruptions are fed from source regions at the base of the crust or deeper in the lunar mantle. According to Wilson and Head (1996), some dikes intruded into the lower crust while others penetrated to the surface, being the sources of extensive outpourings of lava. Thus the surface manifestation of dike emplacement in the crust is depending on the depth below the surface to which the dike penetrates. Wilson and Head (1996) state that if a dike does not propagate near the surface but stalls at greater depth, the strain will be insufficient to cause any dislocation near the surface. If a dike propagates at intermediate depths the strain will cause extensional deformation, eventually leading to graben formation. On the contrary, if a dike propagates to shallow depth and gains surface access at some points, a subsequent lava effusion will occur and the surface manifestation of the dike will be a fracture at which a dome may form (Jackson et al., 1997). Depending on the magma density relative to the density of the crust and the mantle (Wieczorek et al., 2001), and also on the stress state of the lithosphere, some dikes erupt at the surface while others penetrate to depths shallow enough to produce linear graben.

A dike propagating to the surface erupted lavas that produced extensive mare units at high effusione rates. At the terminal stage of the eruption the mass flux decreased, resulting in the formation of domes by increased crystallisation in the magmas and decreasing temperatures. As discussed qualitatively by Weitz and Head (1999) and shown based on rheologic modelling by Wilson and Head (2003) and by Wöhler et al. (2006), the flatter mare domes were formed by lavas of low viscosity erupting at high effusion rates, favouring a low shield to develop, while steeper domes are favoured by lower mass fluxes and temperatures, resulting in higher viscosities and a high crystalline fraction. By comparing the time scale of magma ascent through a dike with the time scale on which heat is conducted from the magma into the host rock, Wöhler et al. (2007) find evidence that the importance of magma evolution processes during ascent such as cooling and crystallisation increases with lava viscosity. Accordingly, different

degrees of evolution of initially fluid basaltic magma are able to explain the broad range of lava viscosities of five orders of magnitude found for lunar mare domes.

Head and Gifford (1980) provide a qualitative morphological classification scheme for lunar domes. Their classes 1–3 refer to largely symmetric volcanic features resembling terrestrial shield volcanoes, displaying comparably steep flanks (class 1), pancake-like cross-sectional shapes (class 2), and very low flank slopes (class 3). Domes of classes 4 and 5 are associated with mare ridges and lava mantling of pre-existing highland terrain, while classes 6 and 7 describe steep highland domes and complex edifices of irregular outline, respectively. Wöhler et al. (2006) introduce an extension of the definitions of classes 1–3 of the scheme by Head and Gifford (1980). They base the distinction between these shield-like volcanoes on their associated spectral and morphometric quantities. Four classes termed A, B, C, and E describing monogenetic mare domes are established essentially according to the diameter, flank slope, and volume of the dome edifice and the TiO_2 content of its soil. Dome classes D and G denote complex non-monogenetic edifies and highland domes, respectively, thus corresponding to classes 7 and 6 of the scheme by Head and Gifford (1980). The properties of the dome classification scheme by Wöhler et al. (2006) are summarised in Table 1. Lena (2007) formulates this scheme as a flow chart, additionally taking into account the rheologic properties of the dome-forming lava (cf. also Section 6).

4 Observations

4.1 Telescopic CCD imagery

Figs. 4a-c display our telescopic CCD images of the Mare Undarum region. They were taken with telescopes of apertures between 200 and 315 mm. The scale of the images is between 300 and 500 m per pixel on the lunar surface. Due to atmospheric seeing, however, the effective resolution (corresponding to the width of the point spread function) is not much better than 1 km. The images were obtained by digitally acquiring several thousands of video frames. Utilising the Giotto and Registax software packages, the individual frames were registered and averaged in order to increase the signal-to-noise ratio (Baumgardner et al., 2000). All images shown in Fig. 4 are oriented with north to the top and west to the left.

The image shown in Fig. 4a was taken on November 07, 2006, at 00:27 UT (colongitude 126.67°), using a 250 mm Newtonian reflector and a DMK 21AF04 CCD camera. The image shown in Fig. 4b was taken on the same date at 01:36 UT (colongitude 127.25°) using a 315 mm Newtonian reflector and a Lumenera Infinity 2-1M CCD camera. The image shown in Fig. 4c was made on December 06, 2006, at 05:16 UT (colongitude 100.10°) using a 200 mm Newtonian reflector and a DMK 21BF04 CCD camera. In all images, a cluster of five domes is apparent. To our knowledge they are not described in preceding lunar dome catalogues (Jamieson and Rae, 1965; Head and Gifford, 1980; Jamieson and Phillips, 1992; Kapral and Garfinkle, 2005). Fig. 4d displays a perpendicular view on the region, derived from Fig. 4b, in which the domes are marked by dots. Their selenographic coordinates (cf. Table 2) have been

determined with the Lunar Terminator Visualization Tool (LTVT) software package (Mosher and Bondo, 2006).

4.2 Lunar Orbiter and Clementine imagery, soil composition

Fig. 2 displays Lunar Orbiter frame IV-178-H1, taken under oblique illumination, which distinctly reveals the previously mentioned smooth and gently sloping domical structures. The available Apollo hand-held camera images of this region (e. g. AS15-M-0939) were acquired under high solar illumination such that the domes are invisible in them.

Table 3 reports reflectance values derived for the domes and two reference units, relying on the calibrated and normalised Clementine five-band UVVIS reflectance data as provided by Eliason et al. (1999). The extracted Clementine UVVIS data were examined in terms of 750 nm reflectance (albedo) R_{750} and the R_{415}/R_{750} and R_{950}/R_{750} colour ratios. Prior to the Clementine mission, the characterisation of lunar soils was performed based on the analysis of ground-based reflectance spectra (Adams and McCord, 1970; McCord et al., 1972; McCord and Adams, 1973; Burns et al., 1976). Charette et al. (1974) have shown that a high UV/VIS (e. g. R_{415}/R_{750}) ratio corresponds to high TiO_2 content and vice versa. More recently, Gillis and Lucey (2005) found that ilmenite grain size or FeO content may also contribute to the UV/VIS ratio. Hence, although TiO_2 content is monotonously increasing with R_{415}/R_{750} ratio, the correlation is only moderate and the data display a strong scatter. Basically, Gillis and Lucey (2005) establish two linear trends. A first trend with a higher slope is apparent for TiO_2 contents of more than 2 wt% found e. g. in the Mare Tranquillitatis region with R_{415}/R_{750} larger than 0.62, while a distinct second trend valid for smaller R_{415}/R_{750} ratios displays a lower slope and is represented e. g. by several types of soils in Oceanus Procellarum. The R_{950}/R_{750} colour ratio is related to the strength of the mafic absorption band, representing a measure for the FeO content of the soil, and is also sensitive to the optical maturity of mare and highland materials (Lucey et al., 1998).

Fig. 5a shows the locations in the Clementine colour ratio image at which the spectra of the five lunar domes in Mare Undarum were obtained. The reflectance spectra of the domes and further nearby geologic units, including the dark and smooth terrain half-way between Condorcet 3 and Dubiago 3 and the nearby hummocky terrain located between the craters Dubiago and Dubiago V, are shown in Fig. 5b. The sample area amounts to 3×3 km^2. All five examined domes are spectrally red with their low R_{415}/R_{750} ratios of 0.57–0.58, indicating a low TiO_2 content of less than 2 wt% according to Gillis and Lucey (2005). The high R_{950}/R_{750} ratios indicate mature mare soils with a low FeO content, for which Clark and Hawke (1987) find values around 11.4 wt% while the FeO map by Lucey et al. (1998) reveals values somewhat below 10 wt%. Condorcet 1 and 3 are spectrally not distinguishable from the mare-like surface into which they merge, while Dubiago 3 and to a lesser extent also Condorcet 2 and 4 have spectra which are intermediate in reflectance between the sampled dark and smooth mare unit and that of the nearby hummocky terrain, which is of higher reflectance and shows a typical highland signature. The observed intermediate spectral signatures may be due to lateral mixing between mare and highland soils (Li and

Mustard, 2000, 2005), as Mare Undarum is characterised by mare ponds rather than extended plains (cf. Section 7).

5 Morphologic and morphometric dome properties

5.1 Morphology of the domes

The selenographic coordinates of the domes and their lateral dimensions (cf. Table 2) were computed using the LTVT software by Mosher and Bondo (2006), which requires a calibration of the images by identifying several control points in the image. This calibration was performed based on the UCLN 2005 list of control points (Archinal et al., 2006). The coordinates were further refined by superimposing the perpendicular view of our images onto the Lunar Topographic Orthophotomap LTO 63D1.

As visible in Figs. 2 and 4, the surfaces around the domes appear to be smooth. The dome Condorcet 1 is bordered at its north-western rim by an elongated, presumably non-volcanic mountain. Similarly, the dome Dubiago 3 displays a central protrusion which is probably a pre-existing, non-volcanic hill. These domes do not display summit pits, at least not at the resolution of the Lunar Orbiter imagery. We estimated the height of the domes Condorcet 3 and 4 based on shadow length measurements in the oblique illumination view shown in Fig. 4b. For Condorcet 3 and 4, heights of 107 ± 15 m and 270 ± 30 m were obtained, respectively.

5.2 Image-based 3D reconstruction of the domes

Due to the fact that the Lunar Orbiter images were acquired on a photographic film scanned on board the spacecraft, resulting in a nonlinear and unknown relation between incident flux and pixel greyvalue, they are not suitable for 3D reconstruction of lunar surface parts based on photometric methods. Similar problems occur for the high-resolution orbital images taken with hand-held and aerial cameras from the Apollo command modules. What is more, the local solar elevation angles are about 20°–30° for Lunar Orbiter images, while nearly all Clementine images were acquired at low phase angles, resulting in steep illumination angles in the equatorial regions where Mare Undarum is situated. The illumination of the surface is therefore not sufficiently oblique in the available spacecraft imagery to apply photoclinometric methods to the lunar domes in this region.

The Lunar Topographic Orthophotomap (LTO) and Lunar Orthophotomap (LO) series were derived from Apollo 15–17 orbital imagery acquired with metric modified aerial cameras. The elevation contour interval of the LTO maps corresponds to 100 m. Topographic maps have also been generated based on Lunar Orbiter stereo imagery. Rosiek et al. (2007) point out that earlier attempts did not yield satisfactory results due to errors in reconstructing the images from film sections scanned on the spacecraft, leading to linear artifacts in the generated digital elevation maps (DEMs). The recent approach by Rosiek et al. (2007) based on digitised Lunar Orbiter data circumvents these problems, resulting in topographic maps which are essentially free of artifacts but still not as accurate as the LTO data.

The domes in Mare Undarum are incorporated in Lunar Topographic Orthophotomap LTO 63D1 (cf. Fig. 6). The fairly complex structure of the dome Condorcet 1 with an elongated non-volcanic mountain at its north-western rim is clearly revealed by this map. According to the elevation contours, the height of the volcanic edifice amounts to 100–200 m. The domes Condorcet 2 and 3 appear as single contour lines, thus indicating approximate heights of 100 m. For the dome Condorcet 4, the topographic map yields an elevation difference of roughly 200–300 m between its summit and its bottom. These height values, however, are very approximate since the resolution of the topographic map is too low to obtain well-defined values for the elevation of the mare plains surrounding the domes.

The lateral resolution of LTO 63D1 is not sufficiently high to display the 3D shapes of the domes in some detail, while the vertical resolution is too low to yield fairly accurate dome heights. As a consequence, for an in-depth morphometric and subsequent rheologic analysis of the domes, we performed a reconstruction of their 3D shape based on the available telescopic image data, relying on the combined photoclinometry and shape from shading method described in detail by Wöhler et al. (2006). These techniques take into account the viewing direction of the camera, the illumination direction, and the surface normal in order to infer the three-dimensional shape of a surface section from the observed intensity distribution in the image.

The reflectance behaviour of the lunar surface depends on the incidence angle θ_i under which it is illuminated by the sun, corresponding to the angle between the surface normal and the illumination direction, the emission angle θ_e between the surface normal and the observing direction, and the phase angle α between the illumination direction and the observing direction. A physically motivated reflectance model is provided by Hapke (1993), which allows to determine soil parameters like single-scattering albedo, average grain size, soil porosity, or average macroscopic surface roughness based on photometric observations performed under a variety of incident, emission, and phase angles. The complex algebraic form of the Hapke model, however, makes it somewhat difficult to use in the context of photometric 3D surface reconstruction algorithms. A phenomenological reflectance law that fits the reflectance behaviour of the lunar surface equally well as the Hapke model for emission angles below 70° is the Lunar-Lambert law

$$R(\theta_i, \theta_e, \alpha) = a \left[2L(\alpha) \frac{\cos\theta_i}{\cos\theta_i + \cos\theta_e} + (1 - L(\alpha)) \cos\theta_i \right] \tag{1}$$

(McEwen, 1991). The Lunar-Lambert reflectance (1) is a weighted sum of the Lambert reflectance (the second term in the sum), which is proportional to $\cos\theta_i$ and describes perfectly diffuse scattering, and the Lommel-Seeliger reflectance (the first term in the sum). The factor a denotes the surface albedo and is estimated based on the assumption that the mean slope across the reconstructed surface part is zero. McEwen (1991) tabulates the phase angle dependent weight parameter $L(\alpha)$ over the complete range of phase angles between 0° and 180° by fitting Eq. (1) to the Hapke model.

For regions near the centre of the lunar disk observed under oblique illumination ($\cos\theta_i \ll 1$) and perpendicular view ($\cos\theta_e$ close to 1), it is pointed out by Wöhler and Hafezi (2005) that the Lunar-Lambert reflectance function remains very similar to the Lambert reflectance function largely independent of the value of the weight factor

$L(\alpha)$. In contrast, near the limb of the lunar disk the deviations from Lambertian reflectance become important. For the low phase angles between 10° and 20° under which the telescopic images shown in Fig. 4 were acquired, McEwen (1991) gives a value of $L(\alpha) = 0.9$ for the lunar macroscopic surface roughness estimated by Warell (2004). Accordingly, under oblique viewing and illumination angles and low phase angles the reflectance behaviour of the lunar surface largely obeys the Lommel-Seeliger law, i. e. the dependence of the surface reflectance on the incidence angle and thus the surface slope is much less pronounced than for Lambertian reflectance – as a note of interest, this reflectance behaviour is responsible for the fact that the full Moon displays no limb darkening. As a consequence, the heights of the domes in Mare Undarum obtained assuming Lambertian reflectance are too low by about a factor of two, compared to the values derived with the Lunar-Lambert reflectance law.

Dome height h and flank slope ζ are readily inferred from the resulting DEM, taking into account the effect of the curvature of the lunar surface. Dome diameter D, height h, and flank slope ζ are related by $\zeta = \arctan(2h/D)$. The dome volume V is computed by integrating the DEM over an area corresponding to a circular region of diameter D around the dome centre. If only a part of the dome surface can be reconstructed e. g. due to the presence of shadows cast by nearby hills, the volume is estimated based on a cross-section in east-west direction through the centre of the dome, assuming rotational symmetry. A rough quantitative measure for the shape of the dome is given by the form factor $f = V/[\pi h(D/2)^2]$ (cf. Table 2), where we have $f = 1/3$ for domes of conical shape, $f = 1/2$ for parabolic shape, $f = 1$ for cylindrical shape, and intermediate values for hemispherical shapes. Wöhler et al. (2006) infer a relative accuracy of 10% for the dome height h and of 25% for the volume V.

Based on the image shown in Fig. 4b, we obtain diameters of 10–12 km for all domes examined in this study, a low flank slope of 0.9° for Dubiago 3, moderate slopes of 1.1°–1.8° for Condorcet 1–3, and a steep slope of 2.8° for Condorcet 4. The edifice volume is fairly low for Dubiago 3 (3.0 km^3), moderate (5–10 km^3) for Condorcet 1–3, and amounts to a large value of 15.3 km^3 for Condorcet 4 (cf. Table 2). Our height values are in good correspondence with those obtained for Condorcet 3 and 4 by shadow analysis (cf. Section 5.1) and are also consistent with the very approximate elevation differences derived from LTO 63D1 for the domes Condorcet 1–4. The DEM obtained for the domes Condorcet 2, 3, and 4 is shown in Fig. 7.

6 Modelling of rheologic properties and dike geometries

Wilson and Head (2003) provide a quantitative treatment of dome-forming eruptions of magma onto a flat plane spreading in all directions from the vent. This model estimates the yield strength τ, i. e. the pressure or stress that must be exceeded for the lava to flow, the plastic viscosity η, yielding a measure for the fluidity of the erupted lava, the effusion rate E, i. e. the lava volume erupted per second, and the duration of the effusion process. In the model by Wilson and Head (2003), the magma is treated

as a Bingham plastic with a yield strength of

$$\tau = \frac{0.323\ h^2\ \rho\ g}{D/2} \tag{2}$$

(Blake, 1990). The plastic viscosity η is then estimated by the empirical relation

$$\eta(\tau) = 6 \times 10^{-4}\ \tau^{2.4}, \tag{3}$$

where τ is expressed in Pa and η in Pa s. In Eq. (2), ρ denotes the lava density, for which Wilson and Head (2003) apply a value of 2000 kg/m^3, $g = 1.63$ m s^{-2} the acceleration due to gravity, h the height of the dome, and D its diameter. In their study, Wilson and Head (2003) regard the Gruithuisen and Mairan highland domes, for which they infer a formation from non-basaltic lava of fairly low density, while the domes in Mare Undarum are composed of mare basalts (cf. Section 4.2), which typically have densities higher than 2000 kg m^{-3} (Wieczorek et al., 2001). However, assuming a higher density will increase the viscosity value merely by a constant factor for all domes. For a high magma density of 2800 kg m^{-3}, this factor amounts to 2.2, compared to the values obtained with 2000 kg m^{-3}, which is not too significant when regarding the broad range of viscosities of about six orders of magnitude inferred for lunar mare and highland domes (Wöhler et al., 2006). Hence, we compute the lava viscosities for $\rho = 2000$ kg m^{-3} in order to facilitate a direct comparison of our results to previous studies (Wilson and Head, 2003; Wöhler et al., 2006; Lena et al., 2007; Wöhler et al., 2007).

Wilson and Head (2003) make the assumption that the advance of the front of a lava flow unit is limited by cooling once a critical depth of penetration of the cooled boundary layer into the flow is reached. Relying on this assumption, they derive a relation for the lava effusion rate E which is based on the effective flow thickness $d_f = c_f \cdot h$ of the dome, which is not straightforward to determine. As an approximation, Wilson and Head (2003) set the effective flow thickness to the elevation difference between the dome surface and the surrounding surface half-way between the dome summit and its outer rim. Accordingly, a value of $c_f = 0.7$ is implied by the parabolic shapes assumed for the Gruithuisen and Mairan highland domes. The relation for the effusion rate obtained by Wilson and Head (2003) then corresponds to

$$E = \frac{0.323^{1/2}\ 300\ \kappa\ (D/2)^2}{0.65^{5/2}\ c_f^2\ h}. \tag{4}$$

Here, $\kappa \approx 10^6$ m^2 s^{-1} denotes the thermal diffusivity of the lava. For the domes examined in this study, we have determined the values of c_f based on the reconstructed DEMs (Table 2). Effectively, the effusion rates for lunar mare domes given in previous studies (Wöhler et al., 2006; Lena et al., 2007; Wöhler et al., 2007) have been computed with $c_f^2 = 0.72$ ($c_f = 0.85$), which is realistic due to the flattened or pancake-like cross-sectional dome shapes. As it is unknown if the ad-hoc assumption of measuring c_f half-way between the dome summit and its rim appropriately reflects the effective flow thickness, and as E depends on the square of c_f, we assume that the values for the

lava effusion rate obtained from Eq. (4) may be off by factors of up to about 2. Hence, these values reflect the order of magnitude of E but should not be taken to be very accurate.

The duration T_e of the lava effusion process amounts to

$$T_e = V/E \tag{5}$$

with the edifice volume V determined according to Section 5.2. Eqs. (2)–(5) are valid for domes that formed from a single flow unit (monogenetic volcanoes). Otherwise, the computed values for τ, η, and E are upper limits to the respective true values.

We obtain comparable effusion rates of 89 and 102 $m^3\ s^{-1}$ for the domes Condorcet 1 and 4, respectively. For the domes Condorcet 2 and 3 higher effusion rates of 172 and 309 $m^3\ s^{-1}$, respectively, are inferred. Condorcet 1–3 formed out of lavas with viscosities between about 7×10^4 Pa s and 5×10^5 Pa s over periods of time between 0.5 and 3.4 years (cf. Table 4). Condorcet 4 is quite different with respect to its morphometric properties and the conditions under which it formed. It originates from lavas of a high viscosity of 5.3×10^6 Pa s, erupting over a comparably long period of time of 4.8 years. The dome Dubiago 3 is very similar in its appearance and also its morphometric properties (moderate to large diameter, low flank slope below 1°) to the intrusive dome immediately north of the large intrusive Valentine dome, located on the western edge of Mare Serenitatis, with $D = 11$ km and $\zeta = 0.8°$ (Lena et al., 2006b; Wöhler et al., 2006). Due to the limited image resolution and the difficult viewing geometry it remains unclear if Dubiago 3 is of effusive or of intrusive origin. Naturally, the rheologic properties derived for this dome, indicating formation from low-viscosity lava erupting at a high effusion rate over a short period of time of three months, are only valid under the assumption of a formation by lava effusion.

As shown by Wilson and Head (2003), the inferred rheologic properties can be used to model the magma rise speed U and the geometry of the dike through which the magma ascended, given by the dike width W and the length L. We will only give a short outline of this model since it has been described in detail by Wilson and Head (2003) and by Wöhler et al. (2007). The three parameters U, W, and L are related to the effusion rate E by

$$E = UWL. \tag{6}$$

The magma rise speed U is found by balancing the vertical pressure gradient dp/dz driving the magma upwards (see below) against the friction at the dike wall, where the yield strength τ has to be overcome before ascending motion can occur:

$$U = \frac{W^2}{12\eta}\left[\frac{dp}{dz} - \frac{2\tau}{W}\right]. \tag{7}$$

Rubin (1993a) has shown by modelling a pressurised dike propagating in a linear viscoelastic medium that the values of W and L are not independent of each other but that their ratio L/W depends on the lava viscosity η. In that model, the ratio p_0/G between the magma pressure p_0 and the elastic stiffness G of the host rock is an important parameter, which lies in the range between 10^{-4} and 10^{-3} (Rubin, 1993a) and

typically amounts to $10^{-3.5}$. In the elastic domain, where the viscosity contrast between the host rock and the magma (a broadly accepted value for the "viscosity" of the host rock is 10^{18} Pa s) is larger than about 12–14 orders of magnitude, the ratio L/W is independent of the magma viscosity and increases approximately linearly with decreasing value of p_0/G. For higher magma viscosities the magma and the host rock are treated as two viscous media, and the value of L/W decreases strongly with increasing magma viscosity. Combining the results of the viscoelastic model by Rubin (1993a) with Eqs. (6) and (7) yields a relation for the dike width W which needs to be computed numerically (cf. also Wöhler et al., 2007).

An important parameter for modelling the geometry of lunar feeder dikes is the vertical pressure gradient dp/dz. Most petrologic models of lunar basaltic magmas suggest an origin by partial melting at 200–400 km depth (Ringwood and Kesson, 1976). The classical model of magma ascent through the lunar crust (Head and Wilson, 1992; Wilson and Head, 1996) predicts that basaltic melts are less dense than the lunar mantle but denser than the overlying crust. Hence, without assuming an excess pressure, basaltic diapirs would rise buoyantly through the lunar mantle but stall near the base of the crust at the so-called neutral buoyancy horizon. According to Wilson and Head (1996), the excess pressure required to drive magma to the surface through a dike and to erupt it onto the surface amounts to 21 MPa for a typical, 64 km thick nearside crust, corresponding to a pressure gradient of $dp/dz = 328$ Pa m^{-1}.

A more recent model of basaltic magma ascent by Wieczorek et al. (2001) assumes a dual-layered structure of the lunar crust. It is shown that basaltic magma should be less dense than the material of the lower crust. In places where the upper anorthositic crust was removed by an impact event, basaltic magma could have been driven to the surface by its positive buoyancy alone. These findings are supported by estimates of the thickness of the lower and the upper crust based on the analysis of gravity anomalies (Wieczorek et al., 2006), indicating that mare basalts are present where the upper crust is found to be absent. In this model, the driving pressure gradient is given by $dp/dz = g\Delta\rho$, where $\Delta\rho$ denotes the density difference between the ascending magma and the crustal material.

At this point, however, we do not need to determine which model is "correct". For basaltic magmas of low TiO_2 content (as found in the Mare Undarum region) at liquidus temperature, Wieczorek et al. (2001) derive a density difference of $\Delta\rho \approx 200$ kg m^{-1}, implying a vertical pressure gradient of $dp/dz \approx 320$ Pa m^{-1}. This value is nearly identical with the one suggested by Wilson and Head (1996). Hence, we have assumed their value of $dp/dz = 328$ Pa m^{-1} to determine the magma rise speeds and dike geometries for the domes in Mare Undarum. The modelling results are summarised in Table 4.

7 Discussion

The oldest materials visible in the Mare Undarum region are those from the impact that produced the Crisium Basin, a multi-ring structure formed 4.05–4.13 Ga ago. The outermost rings are identified by Spudis (1993) as structures of 1080 and 1600 km di-

ameter, respectively, having scarp-like morphologies. Mare Undarum is situated inside the 1080 km ring. During a period of several hundred million years, partial melting occurred at depth in the lunar mantle due to heat released by radioactive decay of elements like potassium, uranium, and thorium (Ringwood and Kesson, 1976). These melts tracked up faults created by the shock wave from the Crisium impact and resulted in the deposition of lava within the basin itself and in peripheral troughs around the basin (Spudis, 1993).

Mare Undarum is a mare patch located outside the main rim of the Crisium impact basin but concentric to Mare Crisium, with the mare basalts being of Upper Imbrian age (Olson and Wilhelms, 1974). The earliest lavas visible in Mare Undarum are those of relatively high albedo, described as unit Im1 in the geologic map by Olson and Wilhelms (1974).

The domes Condorcet 1–3 are aligned radial to Mare Crisium. Similarly, domes in the Hortensius/Milichius/T. Mayer region are aligned radial to the Insularum basin and to the Eastern Procellarum basin postulated by De Hon (1979), and a long chain of domes in the northern part as well as three domes in the western part of Mare Tranquillitatis are aligned radial to the Imbrium basin, respectively (Wöhler et al., 2007). It is suggested by Wöhler et al. (2007) that the ascent of dome-forming lavas was guided by the same internal stress fields induced by major basin impacts which also generated crustal fractures and faulting. While terrestrial crustal fractures are mostly due to tectonic processes, systems of crustal fractures on the Moon were generated by major impact events. Basin impacts caused shock waves that propagated through the lunar surface (Spudis, 1993). These shock waves induced faulting in the subsurface bedrock and reactivated faults caused by preceding impact events. Radial and concentric surface manifestations of faulting in the subsurface layers are apparent around several lunar impact basins (Wilhelms, 1987).

Concentric faulting is visible at the surface e. g. as arcuate rilles or, especially in the case of the Crisium basin, as a system of trough rings (Spudis, 1993). Mare Undarum itself is located in one of the major concentric troughs. Radial to a basin, faulting was caused by the initial shock of the basin impact. These faults were covered by ejecta but reactivated later by subsequent impact events. Examples of surface expressions of such processes are the tectonic faults Rupes Cauchy and Rupes Recta and the linear rilles Rima Cauchy, Rima Ariadaeus, and Rima Hyginus, which display a roughly radial orientation with respect to the Imbrium basin (Wilhelms, 1972).

The alignment of the domes Condorcet 1–3 radial to the Crisium basin confirms the hypothesis that the impact-induced stress fields caused by large impact events facilitated the ascent of dikes from the lunar mantle through the crust. As a rule, the fractures are already closed at depths of ~ 20 km (Wieczorek et al., 2001) and thus do not extend as far down as the mantle source zones of most dikes. Hence, we assume that it is the stress field rather than the actual presence of the pre-existing fractures which favoured the formation and ascent of dikes. In the model by Rubin (1993b), the plane of the dike is perpendicular to the direction of minimum compressive stress, leading to dikes following the same paths as pre-existing fractures, gaining surface access at some points, and eventually erupting lava onto the surface (Petrycki and Wilson, 1999; Wilson and Head, 2003). It is intuitive to assume that the shock wave moves

radially outwards from the location of the impact and that the impact-induced stress is thus maximal in the direction radial to the basin centre and minimal in the direction concentric to it. According to the model by Rubin (1993b), this would immediately explain a radial dike orientation. Hence, the orientation of the dome chain consisting of Condorcet 1–3 indicates that dike formation in Mare Undarum was guided by the stress fields induced by the Crisium impact.

Condorcet 1 and 3 are spectrally not distinguishable from the mare-like surface into which they merge, while the domes Condorcet 2 and 4 and Dubiago 3 have spectra which are intermediate in reflectance between the sampled dark and smooth mare unit and the hummocky terrain (cf. Fig. 5 and Table 3). A mechanism to explain the presence of highland components in mare soils and vice versa is lateral mixing due to random impacts of small bodies as suggested by Li et al. (1997) and modelled in more detail by Li and Mustard (2000). They infer the relative fraction of mare and highland soil along mare-highland contacts based on spectral mixture modelling of Clementine UVVIS data and introduce a so-called anomalous diffusion model that fits well the observed relative abundances at distances of up to 10 km from the boundary. The symmetric shapes of the fraction profiles perpendicular to the boundary indicate that the efficiency of vertical mixing by impact cratering, leading to contamination of mare soil by highland material excavated from below the mare basalt, is negligible compared to lateral mixing. Their studies demonstrate that lateral mixing turns out to be efficient enough to distribute a fraction of 20%–30% of exotic components even over distances larger than 100 km (Li and Mustard, 2005). Accordingly, our interpretation for the observed spectral behaviour of Condorcet 2 and 4 and Dubiago 3 is pronounced lateral mixing. A possible alternative explanation for the highland component in the soils of these domes is the assimilation of crustal wallrock into the ascending magma, but we will show later in this section why assimilation is unlikely to occur under the eruption conditions and dike geometries encountered for the domes in Mare Undarum.

In the classification scheme by Head and Gifford (1980), the domes Condorcet 1–4 are of class 1 while Dubiago 3 is of class 3. Condorcet 1 and Dubiago 3 have small positive reliefs on their surfaces, well visible in the Lunar Orbiter image in Fig. 2. They likely represent pre-existing small peaks surrounded by the domes.

Based on the spectral and morphometric data obtained in this study, the steeper dome Condorcet 4 clearly belongs to class B_1 in the scheme introduced by Wöhler et al. (2006) and later refined by Lena (2007), while its neighbour Condorcet 2 with its low flank slope and rather low edifice volume belongs to class B_2. The dome Condorcet 1 is of class B_2 with some tendency towards class C_1, while the low dome Condorcet 3 with its still lower flank slope, lower edifice volume, and longer duration of the effusion process is a typical class C_1 representative with respect to its morphometric properties. The domes in Mare Undarum consist of lavas of intermediate to high viscosity and low to moderate TiO_2 content, erupting at low to intermediate effusion rates (Tables 1 and 2). If the effusion process continues over a long period of time, steep flank slopes and high edifice volumes may occur as in the case of Condorcet 4 (class B_1), while short periods of effusion result in lower edifices of lower volume, as it is the case for the two domes Condorcet 1 and 2 (class B_2). Condorcet 3, which belongs to class C_1, shows a shallow flank slope mainly due to the low viscosity of the lava from which it formed

(6.8×10^4 Pa s) and the high lava effusion rate (309 m^3 s^{-1}). The dome Dubiago 3 can be assigned to class C_1 according to its morphometric properties. A still lower viscosity, higher effusion rate, and shorter duration of the effusion process than for Condorcet 3 are obtained for Dubiago 3 (cf. Table 4) if we assume that it is of effusive origin. However, this dome is morphometrically very similar to the intrusive dome north of the Valentine dome situated at the western border of Mare Serenitatis, which is described by Wöhler et al. (2006) and in more detail by Lena et al. (2006b). Based on the available observational data we cannot determine if Dubiago 3 is of effusive or of intrusive origin.

Wöhler et al. (2007) establish three rheologic groups of effusive lunar mare domes. These groups differ from each other by their rheologic properties and associated dike dimensions, where the basic discriminative parameter is the lava viscosity η. The first group, R_1, is characterised by lava viscosities of 10^4–10^6 Pa s, magma rise speeds of 10^{-5}–10^{-3} m s^{-1}, dike widths around 10–30 m, and dike lengths between about 30 and 200 km. The domes Condorcet 1–3 belong to this rheologic group, also Dubiago 3 if it is an effusive dome. Other representatives of rheologic group R_1 are the domes of intermediate to large diameter and intermediate flank slope in the Hortensius/Milichius/T. Mayer region. Rheologic group R_2 is characterised by low lava viscosities between 10^2 and 10^4 Pa s, fast magma ascent ($U > 10^{-3}$ m s^{-1}), narrow (W = 1–4 m) and short (L = 7–20 km) feeder dikes. The very low domes in northern and western Mare Tranquillitatis, which all formed from spectrally blue lavas of fairly high R_{415}/R_{750} ratio and thus increased TiO_2 content, are typical representatives of this rheologic group. None of the examined domes found in Mare Undarum belongs to group R_2, presumably due to the low TiO_2 content of the spectrally red mare soil in this region. The third group, R_3, is made up of domes which formed from highly viscous lavas with $\eta = 10^6$–10^8 Pa s, ascending at very low speeds of 10^{-6}–10^{-5} m s^{-1} through broad dikes of several tens to 200 m width and 100–200 km length. The dome Condorcet 4 is a typical representative of rheologic group R_3.

According to Wieczorek et al. (2006), the total crustal thickness in the Undarum region amounts to 55 km while the thickness of the upper crust corresponds to 35 km. If it is assumed that the vertical extension of a lunar dike is comparable to its length L (Jackson et al., 1997), the magma which formed the examined domes in Mare Undarum originated in the upper lunar mantle, well below the crust. A possible exception is Dubiago 3 as the magma reservoir of its feeder dike was situated in the lower crust, provided that this dome is an effusive construct.

The magma rise speeds and dike geometries inferred for the domes in Mare Undarum indicate that vertical mixing by assimilation of wallrock into the ascending magma is not a likely process to explain the observed highland component in the spectral signatures of the effusive domes Condorcet 2 and 4 (in the case of Dubiago 3, assimilation cannot have influenced the spectral appearance of the dome surface already due to its mode of formation, if this dome is assumed to be of intrusive origin). For the rheologic groups R_1 and R_3, to which the Undarum domes belong, the duration of magma ascent is between one and two orders of magnitude higher than the time scale of magma cooling in the dike (Wöhler et al., 2007). Numerical simulations (Carrigan et al., 1992; Wöhler et al., 2007) show that under these "quasi-stationary" conditions the magma

temperature at the border of the dike nearly instantaneously drops down to a value near the average between the host rock temperature and the magma temperature in the middle of the dike. It is demonstrated by Hess (1994) that even in the early lunar history the host rock and the magma were not sufficiently hot to allow melting and subsequent assimilation of significant amounts of crustal wallrock (cf. also Lena et al., 2007).[2]

The domes Condorcet 1–3 are similar to many domes in the Hortensius/Milichius/T. Mayer region in their morphometric and rheologic properties (Wöhler et al., 2006, 2007). The lava plains of Mare Crisium only display a small number of fairly inconspicuous domical structures; at least one rather well-defined dome is situated on the floor of the crater Lick (Kapral and Garfinkle, 2005). A well-examined dome in Mare Crisium is the effusive edifice Yerkes 1, which is situated close to the eastern rim of Mare Crisium, north-east of the crater Yerkes (Wöhler et al., 2006). This dome is remarkably similar to Condorcet 1–3 in its spectral (low R_{415}/R_{750} and high R_{950}/R_{750} spectral ratio) and morphometric properties (cf. Table 5). The close resemblance indicates that the interior conditions during dome formation were similar near the centre of the Crisium basin and in its outer regions.

Lunar mare domes that come close to Condorcet 4 in their morphometric and rheologic properties are two members of the well-studied dome suite north of the crater Hortensius in Mare Insularum, termed Hortensius 5 and 6 by Head and Gifford (1980) and described also by Wöhler et al. (2006). Another mare dome with similar spectral and morphometric properties, examined by Lena et al. (2007), is located south-west of the crater Doppelmayer. The fourth previously known dome of this kind is Herodotus ω situated in Oceanus Procellarum south-west of the crater Aristarchus (Wöhler et al., 2006). These domes are all characterised by comparably steep flank slopes of more than 2.5° and large edifice volumes of about 20–30 km^3 (cf. Table 5). They are of class B_1 in the scheme introduced by Wöhler et al. (2006), who suggest that these domes formed from dikes filled with relatively cool, highly viscous magma nearly saturated with crystals which gained surface access at some points.

The effusion rate for Condorcet 4 of 102 m^3 s^{-1} lies well within the range between 30 and 157 m^3 s^{-1} determined for Hortensius 5 and 6, Herodotus ω, and Doppelmayer 1, while the estimated duration of the effusion process of 4.8 years is somewhat shorter in comparison to Hortensius 5 and 6 (cf. Table 5). Assuming a driving pressure gradient of the magma of $dp/dz = 328$ Pa m^{-1}, we found that the feeder dikes of Hortensius 5 and 6, Herodotus ω, and Doppelmayer 1 have lengths in the range between 145 and 188 km. These values are comparable with the dike length of 178 km estimated for Condorcet 4, indicating an origin of the dome-forming magma well below the lunar

[2]The situation is different for the domes of rheologic group R_2, where the duration of magma ascent is shorter than or comparable to the time scale of magma cooling (Wöhler et al., 2007), resulting in a largely uniform temperature in the dike which is close to the temperature at the dike centre (Carrigan et al., 1992). This leads to a higher wallrock temperature at the dike border than for the domes of rheologic groups R_1 and R_3. However, the R_2 domes known to date do not display highland components in their spectra (Wöhler et al., 2006, 2007). Assimilation is favoured by long durations of the lava effusion process (Spera, 2000), hence in these cases the entrainment of significant amounts of wallrock into the magma has presumably been prevented by the short durations of the effusion process for these domes between typically only a few weeks and three months.

crust. The dike width for Condorcet 4 is slightly lower than the values inferred for the dikes which are supposed to have formed the other four steep and voluminous class B_1 domes. The viscosity of the lava that formed Condorcet 4 of 5.3×10^6 Pa s is comparable to the value derived for Herodotus ω but about a factor of three lower than the viscosities inferred for Hortensius 5 and 6 and Doppelmayer 1. This difference was probably caused by a higher eruption temperature (presumably lower, though, than that of the lavas forming the other examined domes in Mare Undarum) and thus lower crystallinity of the lava.

8 Summary and conclusion

In this study we have examined five lunar domes in Mare Undarum in terms of their spectral and morphometric properties and the eruption conditions encountered during their formation. All five domes have moderate diameters between 10 and 12 km. Condorcet 1–3 are typical effusive mare domes, given their shallow flank slopes and low edifice volumes. They formed from lavas with viscosities around 10^5 Pa s which erupted at high effusion rates between 100 and 300 $m^3\ s^{-1}$ over comparably short periods of time between 0.5 and 3.4 years. Condorcet 1–3 strongly resemble the well-examined dome Yerkes 1 at the western border of Mare Crisium, indicating similar interior conditions during dome formation on regional scales. Condorcet 4 originates from high-viscosity lavas ($\eta = 5.3 \times 10^6$ Pa s) erupting at an effusion rate of 102 $m^3\ s^{-1}$ over a relatively long period of time of 4.8 years. According to its different character (large volume and steep flank slope of 2.8°), the magma rise speed was 1–2 orders of magnitude lower than for Condorcet 1–3, probably due to a lower lava temperature and thus an increased degree of crystallisation during magma ascent. Lunar mare domes that come close to the dome Condorcet 4 in their morphometric and rheologic properties are the two members Hortensius 5 and 6 of the well-studied dome suite in Mare Insularum, the dome Doppelmayer 1 located south-west of the crater Doppelmayer south of Mare Humorum, and Herodotus ω in Oceanus Procellarum. Like Condorcet 4, these domes have flank slopes steeper than 2.5° and high edifice volumes around 20–30 km^3. In contrast to Condorcet 1–4, the dome Dubiago 3 is characterised by morphometric properties that suggest an intrusive origin.

Condorcet 1 and 3 are spectrally not distinguishable from the mare soil of low TiO_2 content into which they merge, while the domes Condorcet 2 and 4 and Dubiago 3 have a spectrum that is intermediate in reflectance between the sampled dark and smooth mare unit and that of the hummocky terrain. This observation is attributable to lateral mixing due to random impacts of small bodies. The alignment of the domes Condorcet 1–3 radial to the Crisium basin suggests their formation by a single radially oriented feeder dike, indicating that the impact-induced stress field facilitated and guided the ascent of dikes from the lunar mantle through the crust. The rheologic properties inferred for Condorcet 1–3 indicate that their common feeder dike had a width of 23 m and a length of 103 km. In this context, the large trough concentric to Mare Crisium in which Mare Undarum is situated is another expression of the stress field building up after the basin impact. Compared to Condorcet 1–3, Condorcet 4

was formed by a considerably wider feeder dike ($W = 127$ m) with a length of 178 km. Assuming a vertical dike extension comparable to the dike length, it follows that for Condorcet 1–4 the dome-forming magma originated in the upper lunar mantle, given the crustal thickness of 55 km in the Mare Undarum region.

Future work will include an extension of our analysis to further effusive mare domes in regions close to the limb of the apparent lunar disk. Such studies may help to gain more detailed insight into the global and regional internal geologic processes responsible for the formation of the observed various types of lunar mare domes.

Acknowledgements: We wish to thank Bob Pilz for contributing the telescopic CCD image of Mare Undarum shown in Fig. 4c.

References

[1] Adams, J. B., McCord, T. B., 1970. Remote sensing of lunar surface mineralogy: implication from visible and near infrared reflectivity of Apollo 11 samples. Proc. Apollo 11 Lunar Sci. Conf., 1937–1945.

[2] Archinal, B. A., Rosiek, M. R., Kirk, L. K., and Redding, B. L., 2006. The Unified Lunar Control Network 2005. US Geological Survey Open-File Report 2006-1367 (Ver. 1.0). `http://pubs.usgs.gov/of/2006/1367/`

[3] Baldwin, R. B., 1963. The Measure of the Moon. Univ. of Chicago Press, Chicago, 390–394.

[4] Baldwin, R. B., 1974. Was there a "Terminal Lunar Cataclysm" 3.9–4.0 $\times$ 10^9 years ago. Icarus 23, 157–166.

[5] Baumgardner, J., Mendillo, M., Wilson, J. K., 2000. A digital high definition imaging system for spectral studies of extended planetary atmospheres, 1. Initial result in white light showing features on the hemisphere of Mercury unimaged by Mariner 10. Astronomical Journal 119, 2458–2464.

[6] Blake, S., 1990. Viscoplastic models of lava domes. In: J. Fink (ed.), Lava Flows and Domes: Emplacement Mechanisms and Hazard Implications, IAVCEI Proc. on Volcanology, vol. 2, Springer-Verlag, New York, 88–128.

[7] Burns, R. G., Parkin, K. M., Loeffler, B. M., Leung, I. S., Abu-Eid, R. M., 1976. Further characterization of spectral features attributable to titanium on the moon. Lunar Planet. Sci. VII, 2561–2578.

[8] Carrigan, C. R., Schubert, G., Eichelberger, J. C., 1992. Thermal and dynamical regimes of single- and two-phase magmatic flow in dikes. J. Geophys. Res. 97(B12), 17377–17392.

[9] Cattermole, P., 1996. Planetary Volcanism. 2nd ed., John Wiley and Sons Ltd., Chichester.

[10] Charette, M. P., McCord, T. B., Pieters, C. M., Adams, J. B., 1974. Application of remote spectral reflectance measurements to lunar geology classification and determination of titanium content of lunar soils. J. Geophys. Res. 79, 1605–1613.

[11] Clark, P. E., Hawke, B. R., 1982. The relationship between geology and geochemistry in the Undarum/Spumans/Balmer region of the moon. Lunar Planet. Sci. XIII, 111–112.

[12] Clark, P. E., Hawke, B. R., 1987. The relationship between geology and geochemistry in the Undarum/Spumans/Balmer region of the moon. Earth, Moon, and Planets 38, 97–112.

[13] De Hon, R. A., 1975. Mare Spumans and Mare Undarum: Mare thickness and basin floor. Proc. 6th Lunar Sci. Conf., 2553–2561.

[14] De Hon, R. A., 1979. Thickness of the western mare basalts. Lunar Planet. Sci. X, 2935–2955.

[15] De Hon, R. A., Waskom, J. D., 1976. Geologic structure of the eastern mare basins. Proc. 7th Lunar Sci. Conf., 2729–2746.

[16] Eliason, E., Isbell, C., Lee, E., Becker, T., Gaddis, L., McEwen, A., Robinson, M., 1999. Mission to the Moon: the Clementine UVVIS global mosaic. PDS Volumes USA NASA PDS CL 4001 4078. `http://pdsmaps.wr.usgs.gov`

[17] Gillis, J. J., Lucey, P. G., 2005. Evidence that UVVIS ratio is not a simple linear function of TiO2 content for lunar mare basalts. Lunar Planet. Sci. XXXVI, abstract #2252.

[18] Hapke, B., 1993. Theory of reflectance and emittance spectroscopy. Cambridge University Press, Cambridge, UK.

[19] Head, J. W., Adams, J. B., McCord, T. B., Pieters, C. M., Zisk, S. H., 1978. Regional stratigraphy and geological history of Mare Crisium. In: Merrill, R., Papike, J. (eds.), Mare Crisium: The View from Luna 24, 43–74, Pergamon Press, New York.

[20] Head, J. W., Wilson, L., 1992. Lunar mare volcanism: Stratigraphy, eruption conditions, and the evolution of secondary crusts. Geochim. Cosmochim. Acta 56, 2155–2175.

[21] Head, J. W., Gifford, A., 1980. Lunar mare domes: classification and modes of origin. The Moon and Planets 22, 235–257.

[22] Hess, P., 1994. Petrogenesis of lunar troctolites. J. Geophys. Res. 99(E9), 19083–19093.

[23] Horn, B. K. P., 1989. Height and Gradient from Shading. MIT technical report 1105A. `http://people.csail.mit.edu/people/bkph/AIM/AIM-1105A-TEX.pdf`

[24] Jackson, P. A., Wilson, L., Head, J. W., 1997. The use of magnetic signatures in identifying shallow intrusions on the moon. Lunar Planet. Sci. XXVIII, abstract #1429.

[25] Jamieson, H. D., Rae, W. L., 1965. The Joint A.L.P.O.-B.A.A. Dome Project. J. Brit. Astron. Assoc. 75, 310–314.

[26] Jamieson, H. D., Phillips, J. H., 1992, Lunar Dome Catalog (April 30, 1992 Edition), Strolling Astronomer 36(3), 123–129.

[27] Kapral, C., Garfinkle, R., 2005. GLR Lunar Dome Catalog. `http://www.glrgroup.org/domes/kapralcatalog.htm`

[28] Kuiper, G. P., Whitaker, E., Strom, R., Fountain, J., Larson, S., 1967. Consolidated Lunar Atlas. Lunar and Planetary Laboratory, University of Arizona. Digital version edited by E. Douglass, 2003, LPI Contribution no. 1114. `http://www.lpi.usra.edu/resources/cla/`

[29] Lena, R., Wöhler, C., Bregante, M. T., Fattinnanzi, C., 2006a. A combined morphometric and spectrophotometric study of the complex lunar volcanic region in the south of Petavius. J. Royal Astr. Soc. of Canada 100(1), 14–25.

[30] Lena, R., Pau, K. C., Phillips, J., Fattinnanzi, C., Wöhler, C., 2006b. Lunar domes: A generic classification of the dome near Valentine, located at 10.26° E and 31.89° N. J. Brit. Astron. Astron. Assoc. 116(1), 34–39.

[31] Lena, R., Wöhler, C., Phillips, J., Wirths, M., Bregante, M. T., 2007. Lunar domes in the Doppelmayer region: spectrophotometry, morphometry, rheology and eruption conditions. Planetary and Space Science 55, 1201–1217.

[32] Lena, R., 2007. Lunar domes classification and physical properties. Selenology Today 5, 62–78.

[33] Li, L., Mustard, J. F., He, G., 1997. Compositional gradients across mare-highland contancts: The importance of lateral mixing. Lunar Planet. Sci. XXVIII, abstract #1724.

[34] Li, L., Mustard, J. F., 2000. Compositional gradients across mare-highland contacts: Importance and geological implication of lateral transport. J. Geophys. Res. 105(E8), 20431–20450.

[35] Li, L., Mustard, J. F., 2005. On lateral mixing efficiency of lunar regolith. J. Geophys. Res. 110(E11), E11002.

[36] Lucey, P. G., Blewett, D. T., Hawke, B. R. 1998. Mapping the FeO and TiO_2 content of the lunar surface with multispectral imagery. J. Geophys. Res. 103(E2), 3679–3699.

[37] McCord, T. B., Adams, J. B., 1973. Progress in optical analysis of lunar surface composition. The Moon 7, 453–474.

[38] McCord, T. B., Charette, M. P., Johnson, T. V., Lebofsky, L. A., Pieters, C., Adams, J. B., 1972. Lunar spectral types. J. Geophys. Res. 77, 1349–1359.

[39] McEwen, A. S., 1991. Photometric Functions for Photoclinometry and Other Applications. Icarus 92, 298–311.

[40] Mosher, J., Bondo, H., 2006. Lunar Terminator Visualization Tool (LTVT). http://inet.uni2.dk/~d120588/henrik/jim_ltvt.html

[41] Mursky, G., 1996. Introduction to Planetary Volcanism. Prentice Hall, Upper Saddle River.

[42] Neukum, G., Ivanov, B. A., Hartmann, W. K., 2001. Cratering records in the inner solar system in relation to the lunar reference system. In: Hartmann, W. K., Geiss, J., Kallenbach, R. (eds.), Chronology and Evolution of Mars, pp. 53–86, Kluwer Academic Publishers, Dordrecht, Netherlands.

[43] Nunes, P. D., Tatsumoto, M., Unruh, D. M., 1974. U-Th-Pb systematics of some Apollo 17 lunar samples and implications for a lunar basin excavation chronology. Proc. 5th Lunar Sci. Conf., 1487–1514.

[44] Olson, A., Wilhelms, D., 1974. USGS Map I-837. USGS, Flagstaff, Arizona.

[45] Petrycki, J. A., Wilson, L., 1999. Volcanic Features and Age Relationships Associated with Lunar Graben. Lunar Planet. Sci. XXX, abstract #1335.

[46] Ringwood, A. F., Kesson, S. E., 1976. A dynamic model for mare basalt petrogenesis. Proc. 7th Lunar Sci. Conf., 1697–1722.

[47] Rubin, A. S., 1993a. Dikes vs. diapirs in viscoelastic rock. Earth and Planet. Sci. Lett. 199, 641–659.

[48] Rubin, A. S., 1993b. Tensile fracture of rock at high confining pressure: Implications for dike propagation. J. Geophys. Res. 98, 15919–15935.

[49] Rosiek, M. R., Archinal, B. A., Kirk, R. L., Becker, T. L., Weller, L., Redding, B., Howington-Kraus, B., Galuszka, D., 2007. Lunar Mapping with Digitized Apollo and Lunar Orbiter Imagery. International Symposium on Geospatial Databases for Sustainable Development, ISPRS Commission IV/7 "Extraterrestrial Mapping", Goa, India.

[50] Schaeffer, O. A., Husain, L., 1974. Chronology of lunar basin formation. Proc. 5th Lunar Sci. Conf., 1541–1555.

[51] Spera, F. J., 2000. Physical Properties of Magma. In: Sigurdsson, H. (ed.), Encyclopedia of Volcanoes, Academic Press, San Diego, USA.

[52] Spudis, P., 1993. The Geology of Multi-Ring Impact Basins. Cambridge University Press, Cambridge, UK.

[53] Spurr, J. E., 1945. Geology Applied to Selenology, vol. I. Science Press, Lancaster, Pa., USA.

[54] Warell, J., 2004. Properties of the Hermean regolith. IV. Photometric parameters of Mercury and the Moon contrasted with Hapke modeling. Icarus 167(2), 271–286.

[55] Weitz, C. M., Head, J. W., 1999. Spectral properties of the Marius hills volcanic complex and implication for the formation of lunar domes and cones. J. Geophys. Res. 104(E8), 18933–18956.

[56] Wieczorek, M. A., Zuber, M. T., Phillips, R. J., 2001. The role of magma buoyancy on the eruption of lunar basalts. Earth and Planet. Sci. Lett. 185, 71–83.

[57] Wieczorek, M. A., and 15 coauthors, 2006. The Constitution and Structure of the Lunar Interior. Rev. Mineralogy and Geochemistry 60, 221–364.

[58] Wilhelms, D. E., McCauley, J. F., 1971. Geologic Map of the Near Side of the Moon. USGS, Flagstaff, Arizona.

[59] Wilhelms, D. E., 1973. Geologic map of the northern Crisium region. Apollo 17 Preliminary Sci. Report, NASA publication SP-330.

[60] Wilhelms, D. E., El-Baz, F., 1977. Geologic map of the east side of the moon. USGS Map I-948, USGS, Flagstaff, Arizona.

[61] Wilhelms, D. E., 1972. Geologic map of the Taruntius quadrangle of the Moon. USGS map I722, USGS, Flagstaff, Arizona.

[62] Wilhelms, D. E., 1987. The geologic history of the Moon. USGS Prof. Paper 1348, USGS, Flagstaff, Arizona.

[63] Wilson, L., Head, J. W., 1996. Lunar Linear Rilles as Surface Manifestations of Dikes: Theoretical Considerations. Lunar Planet. Sci. XXVII, abstract #1445.

[64] Wilson, L., Head, J. W., 2003. Lunar Gruithuisen and Mairan domes: Rheology and mode of emplacement. J. Geophys. Res. 108(E2), 5012–5018.

[65] Wöhler, C., Hafezi, K., 2005. A general framework for three-dimensional surface reconstruction by self-consistent fusion of shading and shadow features. Pattern Recognition 38(7), 965–983.

[66] Wöhler, C., Lena, R., Lazzarotti, P., Phillips, J., Wirths, M., Pujic, Z., 2006. A combined spectrophotometric and morphometric study of the lunar mare dome fields near Cauchy, Arago, Hortensius, and Milichius. Icarus 183, 237–264.

[67] Wöhler, C., Lena, R., Phillips, J., 2007. Formation of lunar mare domes along crustal fractures: rheologic conditions, dimensions of feeder dikes, and the role of magma evolution. Icarus 189(2), 279–307.

Class	R_{415}/R_{750}	ζ [°]	D [km]	V [km^3]
A	> 0.64	0.3–1.0	5–13	< 3
B_1	0.55–0.64	2.0–5.4	6–15	5–32
B_2	0.55–0.64	1.3–1.9	8–15	2–21
C_1	0.55–0.60	0.6–1.8	13–20	7–50
C_2	0.60–0.64	1.0–2.5	8–17	4–17
D	> 0.64	1.3–1.5	≈ 25	40–67
E_1	0.58–0.62	2.0–4.0	< 6	< 1.2
E_2	0.58–0.62	< 2.0	< 6	< 1.2
G	0.55–0.60	> 6.0	7–30	20–390

Table 1: Spectral and morphometric properties characterising the dome classes as defined by Wöhler et al. (2006, 2007).

Dome	Long. [°]	Lat. [°]	D [km]	h [m]	ζ [°]	V [km^3]	f	c_f
Condorcet 1	70.30	7.05	9.7 ± 0.5	150 ± 20	1.8 ± 0.2	9.5 ± 1.9	0.85	0.94
Condorcet 2	70.30	6.72	10.3 ± 0.5	130 ± 15	1.5 ± 0.2	7.4 ± 1.9	0.68	0.77
Condorcet 3	70.64	6.78	11.2 ± 0.5	110 ± 15	1.1 ± 0.1	5.3 ± 1.3	0.49	0.68
Condorcet 4	70.93	6.67	11.1 ± 0.5	270 ± 30	2.8 ± 0.3	15.3 ± 3.8	0.58	0.65
Dubiago 3	71.30	5.54	11.7 ± 0.5	90 ± 10	0.9 ± 0.1	3.0 ± 0.8	0.31	0.69

Table 2: Morphometric properties of the domes in Mare Undarum.

Location	R_{750}	R_{415}/R_{750}	R_{950}/R_{750}
Condorcet 1	0.1162	0.5808	1.0690
Condorcet 2	0.1200	0.5747	1.0920
Condorcet 3	0.1143	0.5731	1.0826
Condorcet 4	0.1240	0.5751	1.0737
Dubiago 3	0.1376	0.5848	1.0648
Mare reference	0.1156	0.5691	1.0690
Highland reference	0.1530	0.5814	1.0927

Table 3: Essential spectral properties of the domes in Mare Undarum according to Clementine UVVIS imagery (cf. also Fig. 5). The size of the sample area on the lunar surface is 3×3 km^2.

Dome	η [Pa s]	E [m^3 s^{-1}]	T_e [years]	U [m s^{-1}]	W [m]	L [km]	Class
Condorcet 1	4.3×10^5	89	3.4	2.2×10^{-5}	30	133	B_2–C_1
Condorcet 2	1.9×10^5	172	1.4	8.6×10^{-5}	21	94	B_2
Condorcet 3	6.8×10^4	309	0.54	3.6×10^{-4}	14	62	C_1
Condorcet 4	5.2×10^6	102	4.8	6.8×10^{-6}	84	178	B_1
Dubiago 3	2.4×10^4	400	0.24	1.1×10^{-3}	9.0	40	C_1
Condorcet 1–3	2.3×10^5	570	–	2.4×10^{-4}	23	103	–

Table 4: Rheologic properties and dike geometries of the domes in Mare Undarum. The rheologic properties inferred for Dubiago 3 are only meaningful if it is taken to be an effusive dome.

Dome	D [km]	ζ [°]	V [km^3]	η [Pa s]	E [m^3 s^{-1}]	T_e [years]	U [m s^{-1}]	W [m]	L [km]
Yerkes 1	9.6	1.3	4.8	1.0×10^5	146	1.05	1.2×10^{-4}	16	73
Hortensius 5	8.5	5.4	18	6.6×10^7	31	18.3	9.2×10^{-7}	243	145
Hortensius 6	12.5	3.6	32	2.3×10^7	70	14.6	2.8×10^{-6}	157	160
Herodotus ω	14.4	2.5	21	1.3×10^6	157	4.3	1.7×10^{-5}	47	188
Doppelmayer 1	16.8	2.8	34	3.4×10^7	121	8.9	5.7×10^{-6}	127	167

Table 5: Morphometric and rheologic properties of the effusive dome Yerkes 1 in Mare Crisium and the exceptionally large, steep, and voluminous class B_1 domes known to date. Morphometric and rheologic data are adopted from Wöhler et al. (2006) and Lena et al. (2007). The values for U, W, and L were derived in this work for Yerkes 1 and are adopted from Wöhler et al. (2007) and Lena et al. (2007) for the other domes.

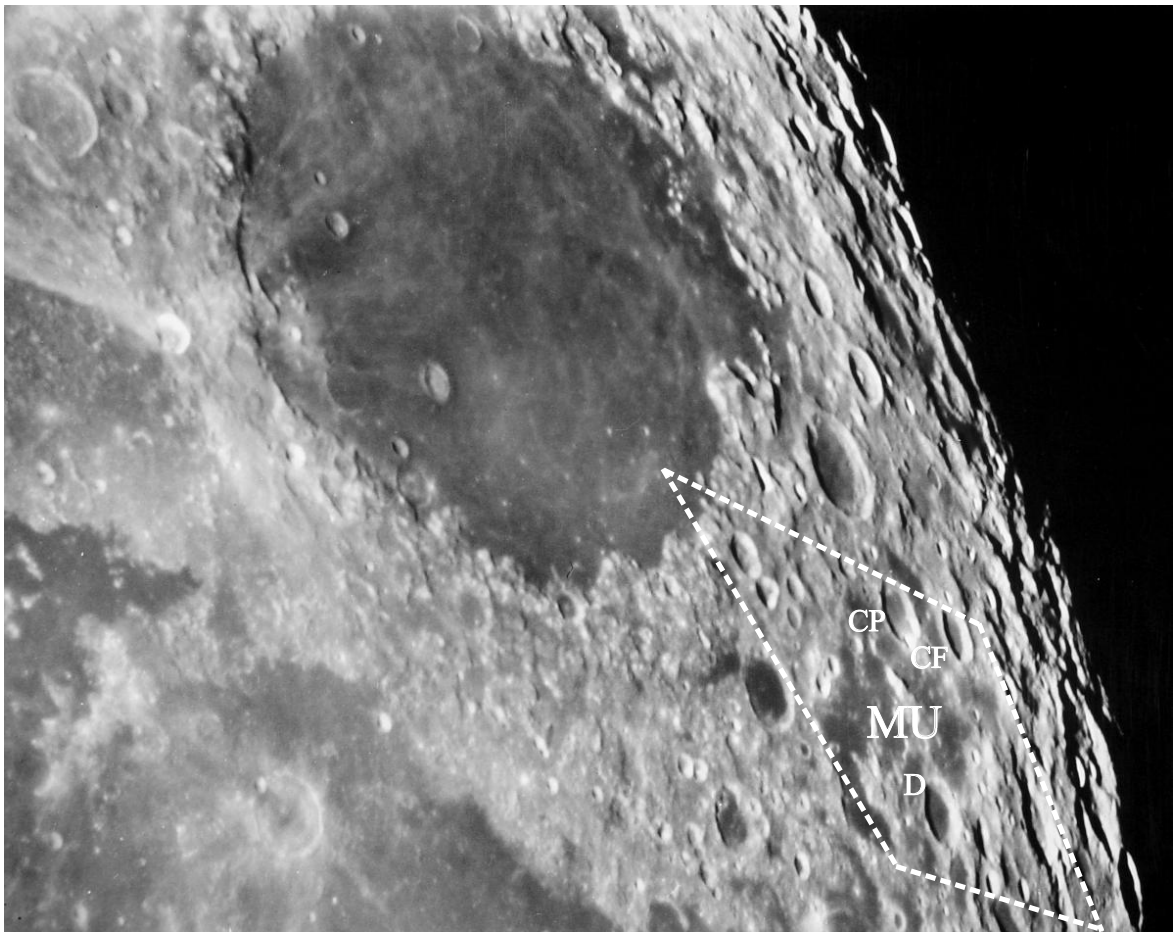

Figure 1: Consolidated Lunar Atlas image D1 (Kuiper et al., 1967), showing an overview of Mare Crisium and Mare Undarum. The white dashed frame indicates the region covered by Fig. 2. MU: Mare Undarum; D: Dubiago; CP: Condorcet P; CF: Condorcet F.

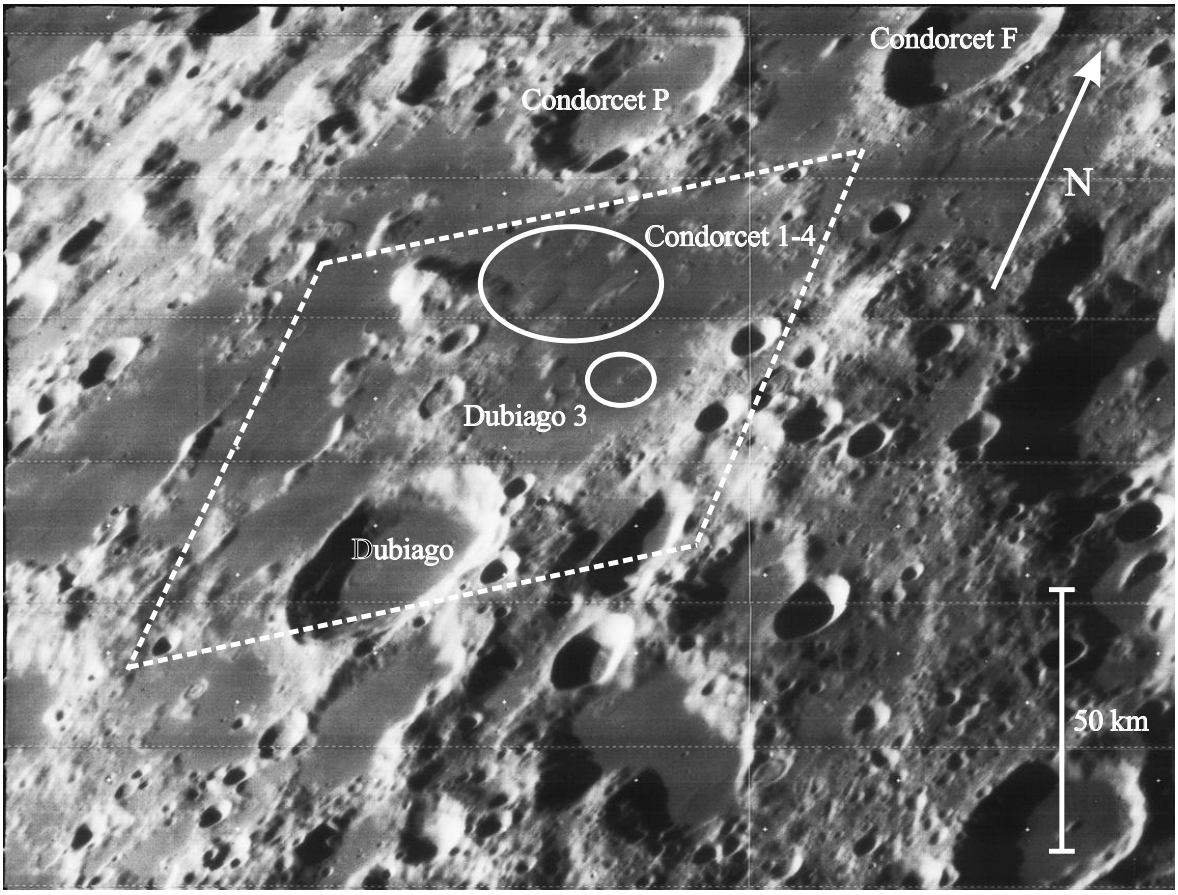

Figure 2: Lunar Orbiter image IV-178-H1, showing an oblique view on Mare Undarum. North is indicated by the arrow in the upper right of the image, undistorted image scale in the lower right. The white dashed frame indicates the region covered by Fig. 4d.

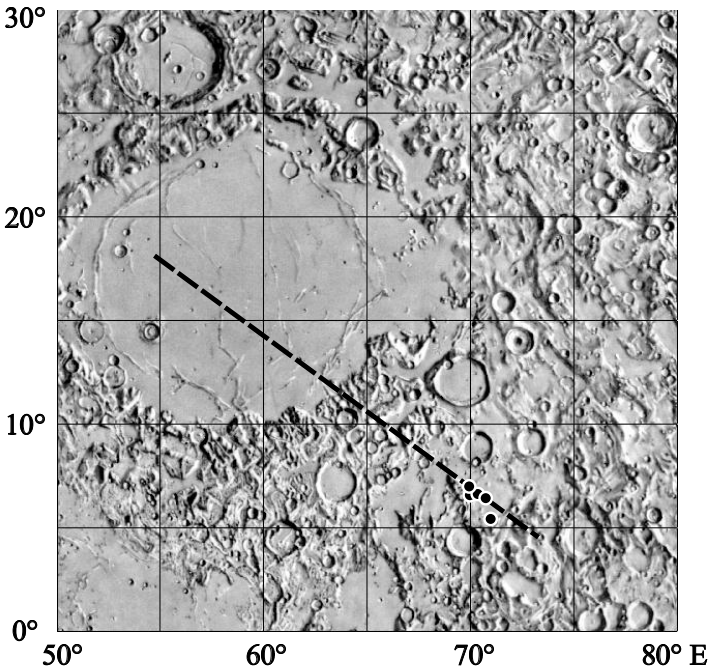

Figure 3: Shaded relief map of the Mare Crisium region, generated by PDSMAPS (`http://pdsmaps.wr.usgs.gov`). The locations of the domes Condorcet 1–4 and Dubiago 3 are indicated by black dots (cf. also Fig. 4d). The alignment of Condorcet 1–3 radial to the Crisium basin is clearly apparent (dashed line).

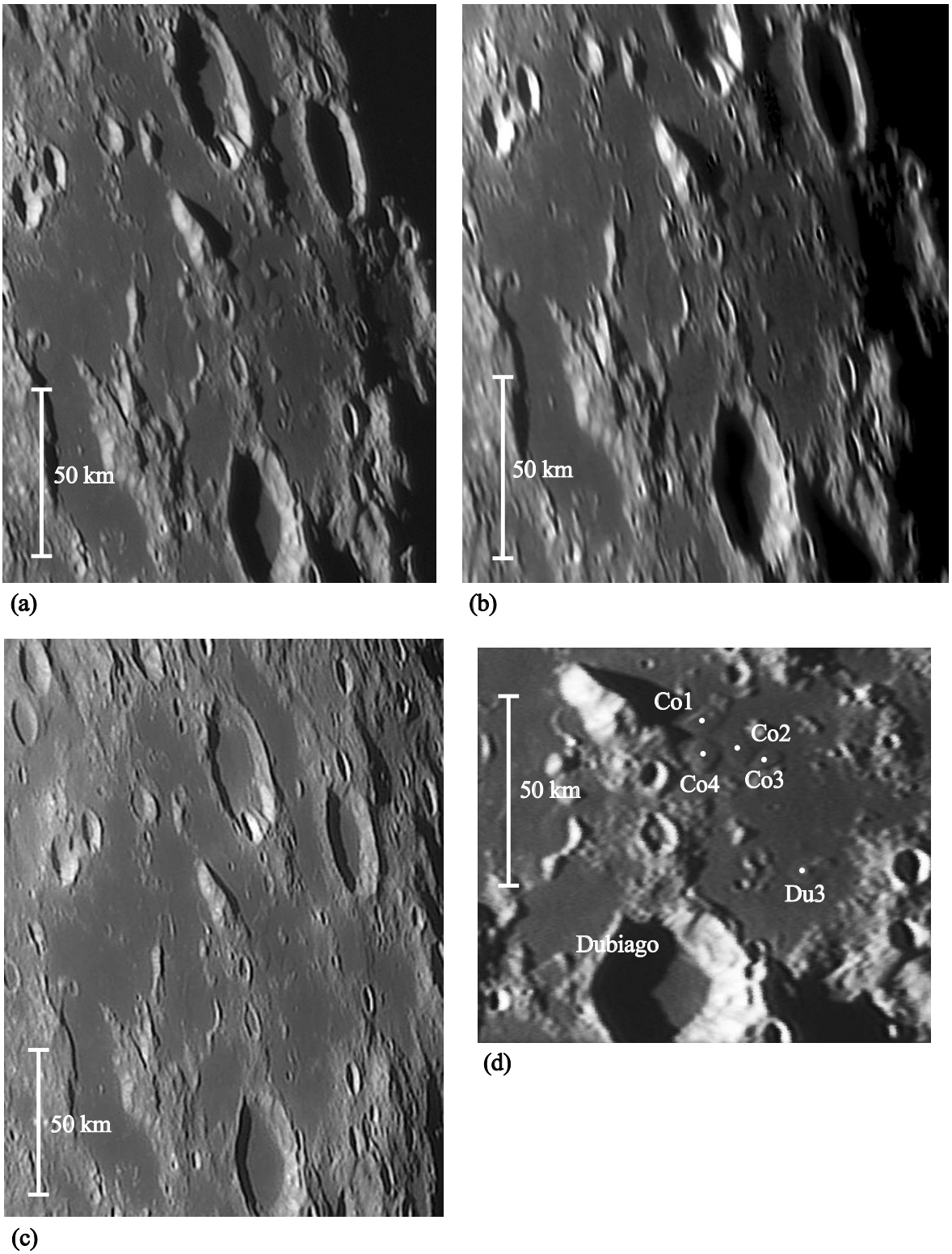

Figure 4: Telescopic CCD images of Mare Undarum. North is to the top and west to the left. Scale bars indicate undistorted image scale. (a)–(b) Mare Undarum under oblique sunset illumination. (c) Mare Undarum under steeper illumation before sunset. Image courtesy Bob Pilz. (d) Image (b) rectified to perpendicular view.

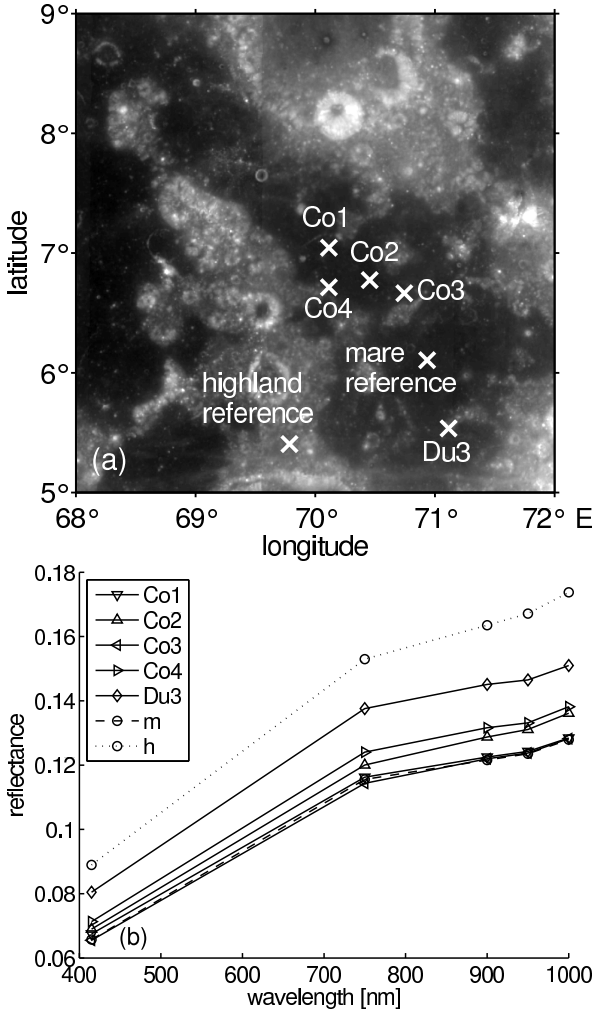

Figure 5: (a) Clementine 750 nm albedo image of eastern Mare Undarum. The locations of the domes examined in this study and the mare and highland reference sites are marked by white crosses. (b) Clementine UVVIS spectra of the indicated locations. The mare reference site is denoted by "m", the highland reference site by "h".

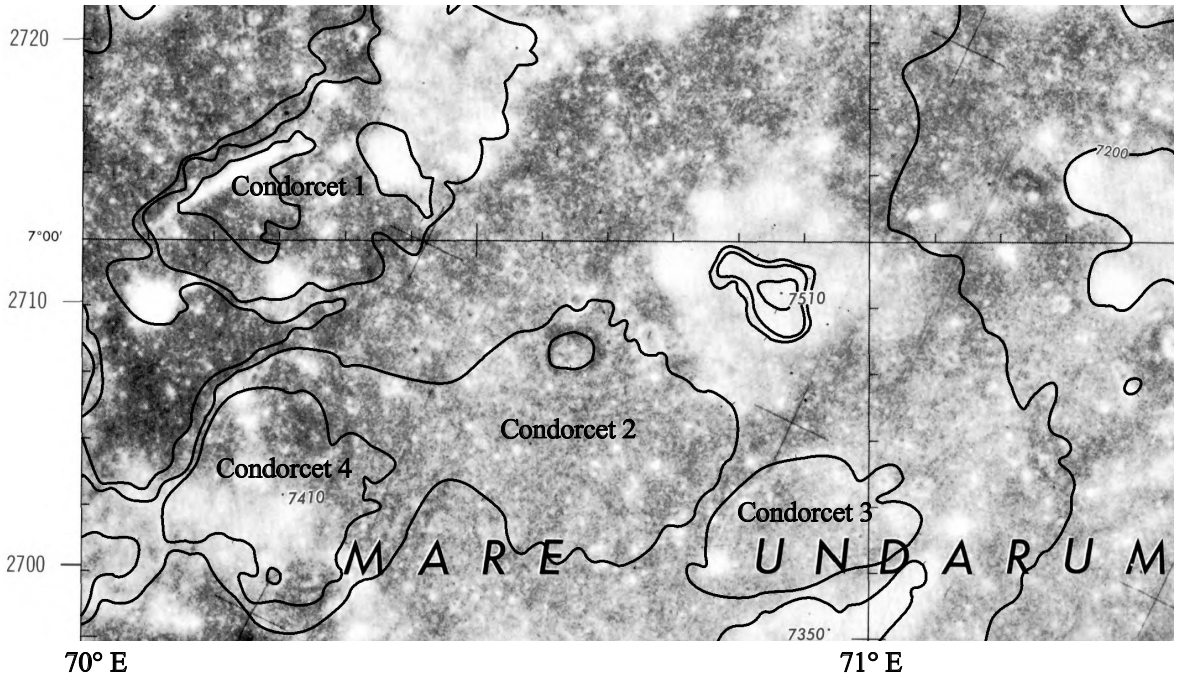

Figure 6: Section of Lunar Topographic Orthophotomap LTO 63D1. The circumferences of the domes Condorcet 2, 3, and 4 as well as the southern and the north-western border of Condorcet 1 appear as contour lines. The contour interval corresponds to 100 m.

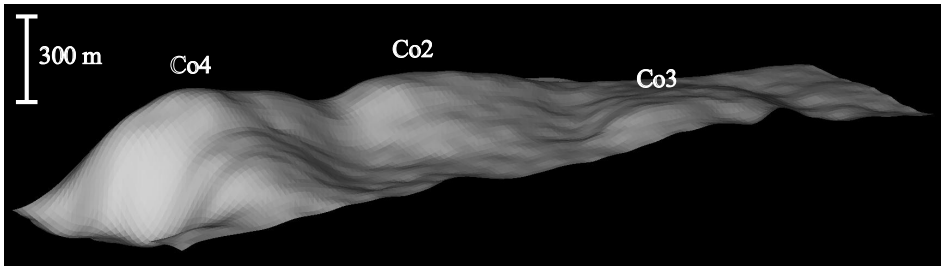

Figure 7: DEM of the domes Condorcet 4, 2, and 3, viewed from south-western direction. The vertical axis is ten times exaggerated.